$1s2p$ resonant inelastic x-ray scattering in α-Fe_2O_3

W. A. Caliebe,* C.-C. Kao, and J. B. Hastings
National Synchrotron Light Source, Brookhaven National Laboratory, Upton, New York, 11973

M. Taguchi† and A. Kotani
Institute for Solid State Physics, University of Tokyo, Roppongi, Minato-ku, Tokyo 106, Japan

T. Uozumi
College of Engineering, University of Osaka Prefecture, Gakuen-cho, Sakai 593, Japan

F. M. F. de Groot
Solid State Physics Laboratory, University of Groningen, Nijenborgh 4 9747 AG Groningen, The Netherlands
(Received 18 March 1998)

We report experimental and theoretical results on the Fe K edge x-ray absorption spectrum and $1s2p$ resonant inelastic x-ray scattering (RIXS) spectra in α-Fe_2O_3. The results are interpreted using an FeO_6^{9-} cluster model with intra-atomic multiplet coupling and interatomic covalency hybridization. The $1s2p$ RIXS is treated as a coherent second-order optical process. It is shown that the double-peak structure in the pre-edge region of Fe K absorption spectrum is due to the cubic crystal-field splitting, and that the intensity of the e_g (t_{2g}) component in the $1s2p$ resonant inelastic spectrum is enhanced by tuning the incident photon energy to the e_g (t_{2g}) component in the absorption spectrum. [S0163-1829(98)08443-4]

I. INTRODUCTION

X-ray absorption spectroscopy (XAS) and x-ray emission spectroscopy (XES) have long played important and complementary roles in the study of the electronic structure of materials. Recently, the increased photon flux and brightness available from undulators and wigglers at synchrotron radiation sources have stimulated a growing number of experimental[1–14] as well as theoretical[15–20] studies exploring resonant inelastic x-ray scattering (RIXS), where x-ray emission spectra are measured as the incident x-ray energy is tuned through an absorption edge of the sample. The second-order nature of the RIXS process offers more degrees of freedom in the design of the experiment selecting appropriate combinations of the type of electric multipole transitions, electronic levels involved in the transitions, as well as combinations of the directions of polarization vector and wave vector of both incident and scattered x rays with respect to the crystal lattice, specific electronic excitations can be studied in greater detail than is possible by either XAS or XES alone.

For wide band solids, the focus of most studies has been on the RIXS process that excites a core electron into the conduction band and measures the valence-band emission spectrum. Within the one-electron approximation, the electron-hole pair in the final state of this RIXS process has been related to the joint density of states between the valence band and conduction band with some success.[2,4,14] However, it is now clear that the effects of core hole in the intermediate states need to be treated properly to account for the detailed line shapes of RIXS spectra,[16,17] and that more theoretical effort is still needed.

For narrow band solids, RIXS at the K,[11] L,[6] and M (Ref. 13) edges of $3d$ transition metals, the M (Ref. 5) and N (Ref. 21) edges of rare-earth elements, and M (Ref. 5) edges of actinides has been exploited to gain information on important high-energy scale parameters, such as the on-site Coulomb interaction energy, charge-transfer energy, as well as related elementary excitations of these correlated electron systems. In all these cases, the cluster models developed for the interpretation of photoemission spectroscopy and x-ray absorption spectroscopy of highly correlated electron systems continue to work very well, and have provided important guidance to the design of experiments.

In this paper, we report a RIXS study of α-Fe_2O_3, hematite. The particular intermediate states of interest are the pre-edge features in the Fe K absorption spectrum of α-Fe_2O_3, and the emission lines of interest are the Fe $K\alpha$ emission lines. In the following, this RIXS process will be referred to as $1s2p$ RIXS.

It is well known that pre-edge features exist in the K absorption spectra of most transition metal compounds. They are usually associated with electronic transitions from the $1s$ core orbital to the localized molecular orbitals of primarily $3d$ character. Since electronic quadrupole transitions ($1s \rightarrow 3d$) are much weaker than electronic dipole transitions, the strength of these pre-edge transitions depends strongly on the local symmetry of the transition metal ion, which affects the degree of admixing between the p-like states with the $3d$ states.[22–24] Consequently, the pre-edge features are a very sensitive analytical tool in the study of the electronic structure of transition-metal compounds. In the case of α-Fe_2O_3, the pre-edge features were assigned to the crystal-field split t_{2g} and e_g states by Dräger *et al.*[23] The presence of quadrupole transitions in these features was confirmed by measuring the wave vector and polarization dependence of the absorption coefficients. The presence of quadrupolar transitions was also independently confirmed recently by the observa-

tion of a forbidden charge reflection in α-Fe_2O_3 by Finkelstein *et al.*[25] However, the ratio of the quadrupolar contribution to the dipolar contribution of these pre-edge features is still not clear.

The reason to study the $K\alpha$ emission line in the RIXS process is that the final state of the process $2p^5 3d^{n+1}$ is identical to that of the $L_{\mathrm{II,III}}$ absorption process. Over the last 10 years, high-resolution soft x-ray absorption spectroscopy has become an important tool in the study of the electronic structure of transition-metal compounds due to the rich multiplet structure of the final states, and the strong linear and circular dichroism associated with them.[26] The possibility to reach the same final states using RIXS permits the unique combination of the spectroscopic information of soft x rays and the flexibility in sample conditions and environments of hard x rays. It is the goal of the present study to investigate this possibility in detail.

The paper is organized as follows: Sec. II describes the experimental arrangement and the experimental results; Sec. III describes the theoretical model; Sec. IV shows calculated results and compares those with experimental results; Sec. V is a summary.

II. EXPERIMENT

The experiment was performed at the X21 hybrid wiggler beamline at the National Synchrotron Light Source. The beamline consists of a four-crystal dispersive Si(220) monochromator with miscut angles of $-16°$, $0°$, $0°$, $+16°$, and a spherically bent Si(333) backscattering analyzer.[27] The energy resolution of the monochromator is 0.2 eV, and the total energy resolution of the experiment is 0.45 eV. The analyzer energy scale was calibrated against that of the monochromator by measuring the elastic scattering line from the sample to ensure that the two energy scales are consistent. The sample used in the experiment was a single-crystal hematite (α-Fe_2O_3) disk oriented in the (111) direction parallel to the momentum transfer. All spectra reported here were measured at 90° scattering angle and in the horizontal plane to reduce scattering background.

Figure 1 shows the Fe *K*-edge absorption spectrum of a powdered α-Fe_2O_3 sample. The spectrum is normalized so that the measured absorption coefficients for photon energies immediately below and well above the absorption edge are the same as the theoretical values.[28] The absorption spectrum agrees very well with data published by Dräger *et al.*,[23] except that the absolute energies of these transitions are 1 eV higher than those reported by Dräger *et al.*[23] Several weak pre-edge peaks are clearly observed. The first two pre-edge peaks, located at 7113.4 and 7114.8 eV, are assigned to the electronic transitions from the Fe 1*s* orbital to the crystal-field split t_{2g} and e_g orbitals.[23] The splitting of 1.4 eV between the two peaks agrees well with both the value of 1.5 eV reported by Dräger *et al.*,[23] and the value of 1.45 eV, obtained from soft x-ray Fe $L_{\mathrm{II,III}}$-edge absorption measurements.[29]

Figure 2 shows three inelastic scattering spectra taken with the incident photon energy tuned to 7113.4 eV (a), 7114.8 eV (b), and 7117.8 eV (c), respectively. The Fe $K\alpha_{1,2}$ fluorescence spectrum of hematite is also included for comparison. The excitation energy of the fluorescence lines was

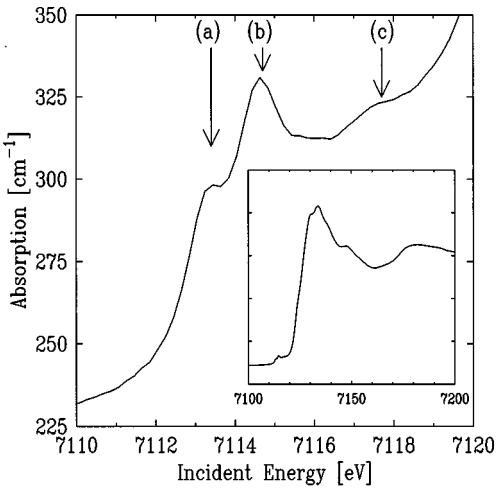

FIG. 1. Fe *K*-absorption edge of powdered α-Fe_2O_3. The pre-edge region is shown in more detail as it is the focus of this paper. The whole edge is shown in the inset. The arrows and labels [(a)–(c)] indicate the incident energies at which the high-resolution emission spectra were measured.

set to $\hbar\omega_1 = 7200$ eV, so that threshold effects are excluded. The $K\alpha_1$ fluorescence line at $\hbar\omega_2 = 6407.3$ eV has an asymmetric Lorentzian line shape with full width at half maximum of about 3.5 eV. All three resonant inelastic spectra have peak positions similar to that of the fluorescence line, but have very different line shapes. In particular, spectra (a) and (b) show much narrower linewidth and additional spectral features.

Figures 3(A) and 3(B) show the same three inelastic-scattering spectra, but as a function of the energy transfer instead of the scattered photon energy. Also, the Fe $L_{\mathrm{II,III}}$ absorption spectrum of hematite is included for comparison in Fig. 3(B). The $L_{\mathrm{II,III}}$ absorption spectrum is shifted down by 0.2 eV to make the peak positions in the inelastic-scattering spectra agree with the peak positions in the absorption spectrum. From Fig. 3, it can be seen that the peak positions of the new spectral features in spectra (a) and (b)

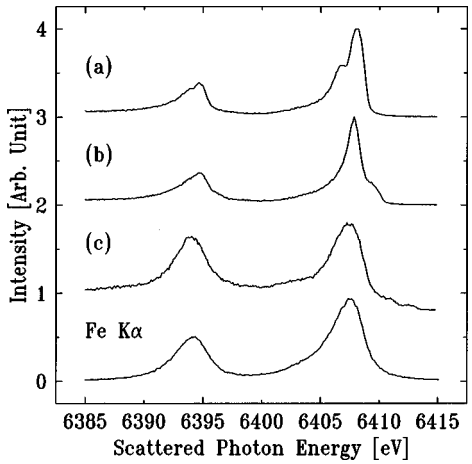

FIG. 2. RIXS spectra as a function of the scattered photon energy for three different energies together with the $K\alpha_{1,2}$ fluorescence lines. The excitation energies are 7113.4 (a), 7114.7 (b) and 7117.7 eV (c) for the RIXS spectra, and 7200 eV for the fluorescence lines, respectively.

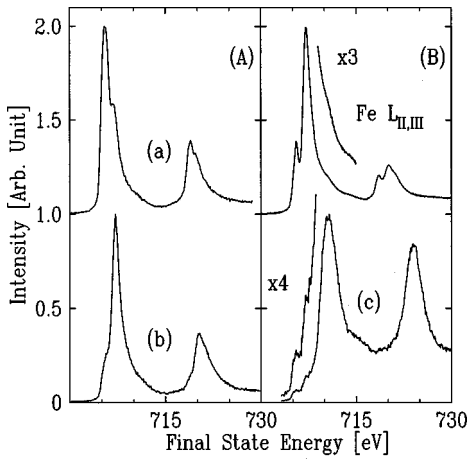

FIG. 3. RIXS spectra as a function of the energy difference of the incident and scattered photon (= final-state energy) together with the $L_{\mathrm{II,III}}$-absorption edge. The excitation energies for the RIXS spectra are the same as in Fig. 2. The spectra (a) and (b) are shown in (A), and spectrum (c) and the $L_{\mathrm{II,III}}$-absorption edge in (B). Two small peaks in the low-energy tail of the main peak in spectrum (c) as well as a small peak in the high-energy side of the Fe L_{III} edge are shown in more detail.

agree well with the main peaks in the $L_{\mathrm{II,III}}$ absorption spectrum. The main peak of spectrum (c), on the other hand, lines up well with the very weak feature at about 711 eV in the absorption spectrum. It should also be noted that there are two very weak peaks with energy transfers between 705–708 eV in spectrum (c), and they also line up well with the main peaks in the $L_{\mathrm{II,III}}$ absorption spectrum.

III. THEORETICAL MODEL

To interpret the RIXS data, we use an FeO_6^{9-} cluster model with O_h symmetry, since the local symmetry around the Fe atom in α-Fe_2O_3 is approximately O_h. The Hamiltonian used in the calculation is given by

$$\begin{aligned} H=&\sum_{\Gamma,\sigma}\varepsilon_{3d}(\Gamma)d^{\dagger}_{\Gamma\sigma}d_{\Gamma\sigma}+\sum_{m,\sigma}\varepsilon_{2p}p^{\dagger}_{m\sigma}p_{m\sigma}+\sum_{\sigma}\varepsilon_{1s}s^{\dagger}_{\sigma}s_{\sigma}\\ &+\sum_{k,\sigma}\varepsilon_{4p}(k)P^{\dagger}_{k\sigma}P_{k\sigma}+\sum_{\Gamma\sigma}\varepsilon_{l}(\Gamma)a^{\dagger}_{\Gamma\sigma}a_{\Gamma\sigma}+\sum_{\Gamma,\sigma}V(\Gamma)\\ &\times(d^{\dagger}_{\Gamma\sigma}a_{\Gamma\sigma}+a^{\dagger}_{\Gamma\sigma}d_{\Gamma\sigma})\\ &+U_{dd}\sum_{(\Gamma,\sigma)\neq(\Gamma',\sigma')}d^{\dagger}_{\Gamma\sigma}d_{\Gamma\sigma}d^{\dagger}_{\Gamma'\sigma'}d_{\Gamma'\sigma'}\\ &-U_{dc}(1s)\sum_{\Gamma,\sigma,\sigma'}d^{\dagger}_{\Gamma\sigma}d_{\Gamma\sigma}(1-s^{\dagger}_{\sigma'}s_{\sigma'})\\ &-U_{dc}(2p)\sum_{\Gamma,m,\sigma,\sigma'}d^{\dagger}_{\Gamma\sigma}d_{\Gamma\sigma}(1-p^{\dagger}_{m\sigma'}p_{m\sigma'})+H_{\mathrm{multiplet}}, \end{aligned} \tag{3.1}$$

where $\varepsilon_{3d}(\Gamma)$ and $\varepsilon_l(\Gamma)$ represent the energies of Fe $3d$ and O $2p$ ligand states, respectively, with the irreducible representation Γ ($=e_g$ and t_{2g}) of the O_h symmetry. The energies ε_{2p} and $\varepsilon_{4p}(k)$ represent the Fe $2p$ and Fe $4p$ states, respectively, where we take into account the finite width of the Fe $4p$ conduction band with the wave vector k beyond the cluster model (the band index is dropped for simplicity). The indices m and σ are the orbital and spin states. $V(\Gamma)$, U_{dd}, $-U_{dc}(1s)$ and $-U_{dc}(2p)$ are the hybridization between Fe $3d$ and O $2p$ ligand states, the Coulomb interaction between Fe $3d$ states, the Coulomb interaction between Fe $3d$ and $1s$ core-hole states, and that between Fe $3d$ and $2p$ core-hole states, respectively. The Hamiltonian $H_{\mathrm{multiplet}}$ describes the intra-atomic multiplet coupling originating from the multipole Coulomb interaction between Fe $3d$ states and that between Fe $3d$ and $2p$ states. The spin-orbit interaction for Fe $3d$ and $2p$ states is also included in $H_{\mathrm{multiplet}}$.

In the pre-edge region of XAS, the Fe $1s$ electron is excited to the $3d$ states by the quadrupole transition. The XAS is given as

$$I_{\mathrm{Q}}(\Omega)=\sum_{m}|\langle m|T_{\mathrm{Q}}|g\rangle|^2\frac{\Gamma_K/\pi}{(\Omega-E_m+E_g)^2+\Gamma_K^2}, \tag{3.2}$$

and $K\alpha$ RIXS is given, using the formula of the coherent second-order optical process, as

$$\begin{aligned} S_{\mathrm{Q}}(\Omega,\omega)=&\sum_{f}\left|\sum_{m}\frac{\langle f|T_{\mathrm{D}}|m\rangle\langle m|T_{\mathrm{Q}}|g\rangle}{E_g+\Omega-E_m-i\Gamma_K}\right|^2\\ &\times\frac{\Gamma_M/\pi}{(E_g+\Omega-E_f-\omega)^2+\Gamma_M^2}, \end{aligned} \tag{3.3}$$

where $|g\rangle$, $|m\rangle$, and $|f\rangle$ are the ground, intermediate and final states of RIXS (eigenstates of the Hamiltonian H) with energies E_g, E_m, and E_f, respectively. It should be noted that the final states of XAS are the same as the intermediate states of RIXS. The incident and emitted photon energies are represented by Ω and ω, respectively. The core-hole lifetime broadening is denoted by Γ_K for the $1s$ core hole and Γ_M for the $2p$ core hole. The operators T_{Q} and T_{D} represent the optical quadrupole transition between Fe $1s$ and $3d$ states and the optical dipole transition between Fe $2p$ and $1s$ states, respectively, and they are written as

$$T_Q=\sum_i\sum_{q=-2}^{2}r_i^2C_q^{(2)}(i), \tag{3.4}$$

$$T_D=\sum_i\sum_{q=-1}^{1}r_iC_q^{(1)}(i). \tag{3.5}$$

Here r_i is the radial coordinate of the ith electron in the system and $C_q^{(k)}(i)$ is the spherical tensor operator. In our calculation of RIXS, it is assumed for simplicity that the spectrum is averaged over all the polarization directions of incident and emitted x rays.

Even in the pre-edge region of XAS, a weak low-energy tail of the dipole transition of the Fe $1s$ electron to the Fe $4p$ conduction band coexists with the quadrupole transition. The XAS due to the dipole transition is given as

$$I_{\mathrm{D}}(\Omega)=\sum_m |\langle m|T_{\mathrm{D}}|g\rangle|^2 \frac{\Gamma_K/\pi}{(\Omega-E_m+E_g)^2+\Gamma_K^2}$$
$$=\int d\varepsilon\rho(\varepsilon)\sum_{m'} |\langle m',k|T_{\mathrm{D}}|g\rangle|^2 \times\frac{\Gamma_K/\pi}{(\Omega-\varepsilon-E_{m'}+E_g)^2+\Gamma_K^2}. \quad (3.6)$$

Here the final state $|m\rangle$ is assumed to be a direct product of a $4p$ state $|k\rangle$ and the remaining system $|m'\rangle$ ($|m\rangle=|m',k\rangle=|m'\rangle|k\rangle$) with the energy $E_m=E_{m'}+\varepsilon_k$, and then the summation over the $4p$ final state is replaced by the integral over ε ($=\varepsilon_k$) with the density of states $\rho(\varepsilon)$. In a similar way, $K\alpha$ RIXS due to the dipole excitation is expressed in the form

$$S_{\mathrm{D}}(\Omega,\omega)=\int d\varepsilon\rho(\varepsilon) \times\sum_{f'}\left|\sum_{m'}\frac{\langle f',k|T_{\mathrm{D}}|m',k\rangle\langle m',k|T_{\mathrm{D}}|g\rangle}{E_g+\Omega-\varepsilon-E_{m'}-i\Gamma_K}\right|^2 \times\frac{\Gamma_M/\pi}{(E_g+\Omega-\varepsilon-E_{f'}-\omega)^2+\Gamma_M^2}, \quad (3.7)$$

where we put $|f\rangle=|f',k\rangle=|f'\rangle|k\rangle$ and $E_f=E_{f'}+\varepsilon_k$. Finally, the total spectra, $I(\Omega)$ and $S(\Omega,\omega)$, are given as

$$I(\Omega)=I_{\mathrm{Q}}(\Omega)+I_{\mathrm{D}}(\Omega), \quad (3.8)$$

$$S(\Omega,\omega)=S_{\mathrm{Q}}(\Omega,\omega)+S_{\mathrm{D}}(\Omega,\omega). \quad (3.9)$$

IV. CALCULATED RESULTS

In order to describe the ground state of our cluster model, we use, as the basis states, the three configurations, $3d^5$, $3d^6L$, and $3d^7L^2$, where L represents a hole in the ligand states. The basis configurations in the intermediate state $|m\rangle$ are $1s3d^6$, $1s3d^7L$ and $1s3d^8L^2$ configurations for the quadrupole-excited states and $1s3d^5 4p$, $1s3d^6L4p$, and $1s3d^7L^2 4p$ configurations for the dipole-excited state. Corresponding to these intermediate states, the basis configurations in the final state $|f\rangle$ are $2p3d^6$, $2p3d^7L$, and $2p3d^8L^2$ configurations (quadrupole) and $2p3d^5 4p$, $2p3d^6L4p$, and $2p3d^7L^2 4p$ configurations (dipole), respectively. The parameter values are as follows: $U_{dc}(1s)=U_{dc}(2p)=7.3$, $V(e_g)=2.3$, $U_{dd}=6.0$, and $\Delta=4.7$ in units of eV, where Δ is the charge-transfer energy defined by the energy difference between $3d^6L$ and $3d^5$ configurations. For the hybridization, we use the empirical relation: $V(e_g)=-2V(t_{2g})$. These parameter values are mainly estimated from the analysis of x-ray photon spectroscopy data. The Slater integrals and the spin-orbit coupling constants that are included in $H_{\mathrm{multiplet}}$ are calculated by Cowan's Hartree-Fock program,[30] and then the Slater integrals are reduced to 85% of the Hartree-Fock values. For the crystal-field splitting, we use $10Dq=0.94$ eV. This value is smaller than $10Dq=1.45$ eV used by Kuiper *et al.*[29] in their analysis of x-ray magnetic linear dichroism, but we explicitly take into account the effect of covalency hybridization whereas they did not. The lifetime broadening of the core hole is taken to be $\Gamma_K=0.6$ eV and $\Gamma_M=0.18$ eV, and the Gaussian broadening to be 0.25 eV half width at half maximum. With the parameter values given above, the ground state is the mixed state of the three configurations with the mixing weights 82.2% ($3d^5$), 17.0% ($3d^6L$), and 0.8% ($3d^7L^2$).

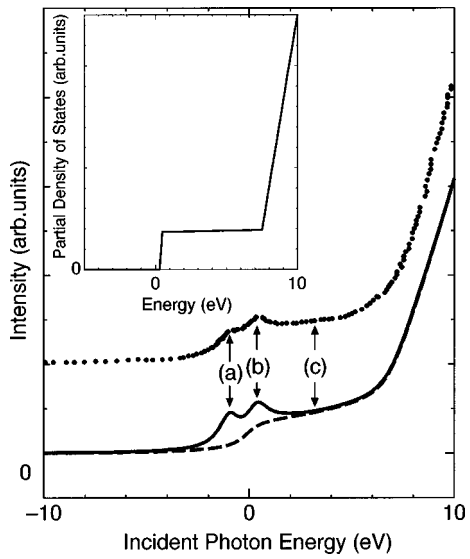

FIG. 4. Calculated Fe K-absorption edge of α-Fe_2O_3 together with the measured data. The dashed line represents the background in the pre-edge region, which stems from dipole transition. The arrows indicate the incident energies for which the emission spectra were measured and calculated (same as in Fig. 1). The inset shows the assumed density of states of the Fe $4p$ conduction band $\rho(\epsilon)$.

The calculated Fe K pre-edge XAS is shown in Fig. 4, together with the experimental result. In this calculation, we assume the density of states of Fe $4p$ conduction band $\rho(\varepsilon)$ as shown in the inset of Fig. 4 so as to reproduce the experimental results, and the relative intensity between the quadrupole and dipole transitions and their relative energy position are taken as adjustable parameters. The energy separation between the quadrupole and the dipole transition is 7 eV (from the center of the quadrupole transition to the steep absorption edge of the dipole transition in Fig. 4), and the intensity ratio between the transitions is 0.07 (integrated intensity ratio within the energy range of -10 to 10 eV in Fig. 4). It is difficult to compare these numbers to published values, which are of the order of 20 eV and 0.01, respectively.[31] These numbers describe the separation and the ratio of the white line to the quadrupole transition, while we take the ratio in the near-edge region.

In the pre-edge region, we can see a double-peak structure with an energy splitting of about 1.4 eV. A schematic energy diagram of the optical transition is shown in Fig. 5. Since the predominant ground-state configuration is $(t_{2g}\uparrow)^3(e_g\uparrow)^2$, we approximately put $|g\rangle=|(t_{2g}\uparrow)^3(e_g\uparrow)^2\rangle$ in Fig. 5. Then, the final states of XAS (intermediate states of RIXS) by the quadrupole transition are $d^\dagger_{t_{2g}\downarrow}s_\downarrow|g\rangle$ and $d^\dagger_{e_g\downarrow}s_\downarrow|g\rangle$, whose energy separation is given by the e_g-t_{2g} splitting, $10Dq$. This explains the double-peak structure. The main effect of the hybridization is to enlarge this energy separation from

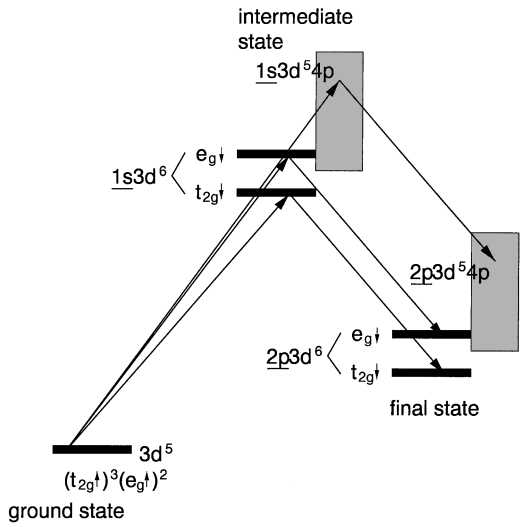

FIG. 5. Energy diagram of the optical transitions, which are observed in the experiment. $1s$ electrons in the ground state ($3d^5$) are excited into either the localized e_g or t_{2g} orbitals ($\underline{1s}3d^6$) or the $4p$ valence band ($\underline{1s}3d^5 4p$) in the intermediate state of RIXS (=final state in XAS). In RIXS, the intermediate state decays into the final states $\underline{2p}3d^6$ or $\underline{2p}3d^5 4p$, respectively.

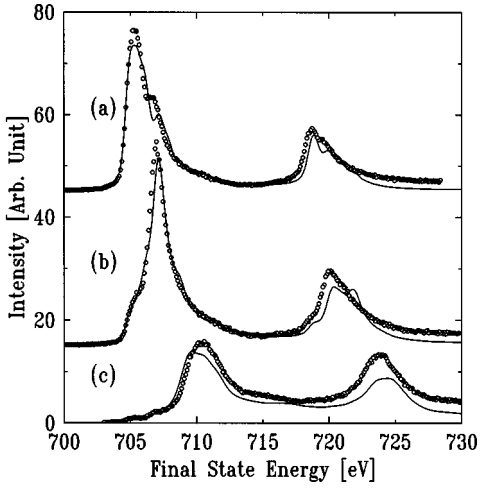

FIG. 6. Calculated RIXS spectra (solid line) as a function of the energy difference of the incident and scattered photon together with the measured spectra (symbols). The energies of the incident photons are the same as in Figs. 2 and 3, and they are labeled accordingly with (a)–(c).

0.94 eV ($=10Dq$) to 1.4 eV. The charge-transfer satellite is too weak to be clearly seen, because the core-hole charge is screened by the photoexcited $3d$ electron in the final state of XAS. The dipole transition contributes to the background absorption in the pre-edge region as shown with the dashed curve in Fig. 4.

Here it should be mentioned that the interpretation of the pre-edge structure observed in various transition-metal compounds is, in general, not well established. If there is a local lattice distortion like a vibrational excitation, which breaks the inversion symmetry around the transition-metal site, the $1s$ to $3d$ transition becomes weakly allowed by the optical dipole transition.[32] Even when the inversion symmetry is not broken, the dipole transition is possible from the $1s$ state to the $3d$ state on a different transition-metal site, if we extend the cluster size. In the case of the Ti K edge in TiO_2 (rutile), for instance, both quadrupole and dipole transitions are shown to give important contributions to the pre-edge structure.[26,33] In the present analysis of the Fe K pre-edge of Fe_2O_3, we can reproduce the experimental double-peak structure by the quadrupole transitions superimposed on the background of the dipole transition, where we have used some assumptions on the $4p$ band density of states and the relative intensity and energy position between the quadrupole and dipole contributions. It will be shown below that the present model with these assumptions can also reproduce the experimental data of $1s2p$ RIXS.

The results of $1s2p$ RIXS calculations are shown in Fig. 6, where the spectra (a), (b), and (c) are obtained by tuning the incident photon energy to the energy positions (a), (b), and (c) in Fig. 3. Here the spectra of the emitted photon are plotted as a function of the energy transfer $\omega-\Omega$. The symbols are the experimental data, the symbol size is a measure for the statistical errors. The solid lines describe the theoretical data. The contributions from the dipolar and quadrupolar transitions are separately shown in Fig. 7 and compared to the sum of both transitions. The model calculation and experimental results are in very good agreement. The two prominent structures separated by about 13 eV originate from the spin-orbit splitting of the $2p$ core level, $2p_{3/2}$ and $2p_{1/2}$. In going from (a) to (b), the energy of the maximum RIXS peak shifts in both $2p_{3/2}$ and $2p_{1/2}$ components by about 1.4 eV in the direction of increasing energy transfer, and from (b) to (c), the maximum peak energy shifts further by about 3 eV on the high energy-transfer side. This is explained as follows: As shown in Fig. 5, the intermediate state $d^\dagger_{t_{2g}\downarrow}s_\downarrow|g\rangle$ [(a) in Fig. 6] decays mainly into the final state $d^\dagger_{t_{2g}\downarrow}p_{m\downarrow}|g\rangle$, and the intermediate state $d^\dagger_{e_g\downarrow}s_\downarrow|g\rangle$ [(b) in Fig. 6] into the final state $d^\dagger_{e_g\downarrow}p_{m\downarrow}|g\rangle$. The energy difference of the two final states is the e_g-t_{2g} splitting (=1.4 eV) again.

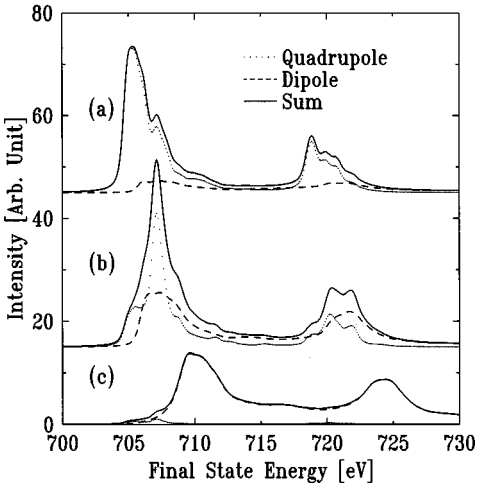

FIG. 7. Comparison of the quadrupolar and dipolar contribution to the calculated RIXS spectra in Fig. 6. The energies are same as in the Figs. 2, 3, and 6. Obviously, the quadrupolar contribution dominates in the spectra (a) and (b), while in (c) the dipolar contribution yields most of the intensity for the peak. The quadrupolar contribution with transitions into the t_{2g} and e_g orbitals is observable as small steps at 705 and 707 eV, respectively.

According to Eq. (3.3), the energy transfer of RIXS is given by the energy difference between the energies E_f and E_g, so that when we go from (a) to (b), the RIXS peak shifts by 1.4 eV. Of course this transition scheme is very crude, and actually the states $d^\dagger_{t_{2g}\downarrow}p_{m\downarrow}|g\rangle$ and $d^\dagger_{e_g\downarrow}p_{m\downarrow}|g\rangle$ are not the eigenstates of the Hamiltonian H, thus they are mixed into each other by the Coulomb interaction between $3d$ and $2p$ states, as well as by the spin-orbit interaction in the $2p$ state. Therefore, we find, in the case of (a) [and (b)], a shoulder structure about 1.4 eV on the high- (and low-) energy side of the main peak in the $2p_{3/2}$ component of RIXS.

Next, we consider the contribution from the dipole excitation, where the intermediate state is $P^\dagger_{k\sigma}s_\sigma|g\rangle$ and the final state is $P^\dagger_{k\sigma}p_{m\sigma}|g\rangle$, as shown in Fig. 6. In the cases of (a) and (b) the excited $4p$ electron stays near the bottom of the $4p$ conduction band, so that the energies of the intermediate and final states are very close to those of the quadrupole excitations. Therefore, we have the contribution from the dipole excitation (dashed curve) to RIXS in the energy-transfer region very close to that of the quadrupole excitation, although the dipole contribution is much weaker than the quadrupole contribution. In the case of (c), on the other hand, the dipole contribution is much stronger than the quadrupole contribution, because the XAS intensity of the dipole transition is much larger than the quadrupole transition. Furthermore, the excited $4p$ electron stays about 3 eV above the bottom of the conduction band corresponding to the increase in the incident photon energy. Therefore, the final state energy of the dipole contribution is about 3 eV higher than the quadrupole contribution, resulting in the shift of the RIXS peak energy by about 3 eV in going from (b) to (c). In the spectrum (c) we can also see weak structures caused by the quadrupole excitation at the same energy-transfer position as in (a) and (b). Note that in the case of (c), the intermediate state of the quadrupole transition occurs as a virtual process with the off-resonance energy of about 3 eV, but that of the dipole transition occurs as a real process because of the continuous energy of the $4p$ conduction band.

V. SUMMARY

In summary, we present a high-resolution Fe K-edge x-ray absorption spectrum and $1s2p$ RIXS spectra of α-Fe_2O_3. The results are interpreted using a cluster model in which intra-atomic multiplet coupling and interatomic hybridization are included explicitly. Very good agreement between the experimental results and the model calculations is achieved in both the XAS spectrum and RIXS spectra.

This study clearly demonstrates that for $3d$ transition metals the $1s2p$ RIXS process can be exploited to obtain spectroscopic information similar to that obtained in $L_{\mathrm{II,III}}$-absorption spectroscopy. Since both incident and scattered photons are hard x rays, it opens the opportunity for *in situ* spectroscopic studies of transition-metal ions, complexes, and clusters in biological and other systems that are not vacuum compatible.

Moreover, polarization and wavevector dependence in the $1s2p$ RIXS spectra can be further exploited. For example, the enhancement of the e_g (t_{2g}) component in the RIXS spectra could be even greater by a proper choice of the incident polarization vector with respect to the crystal orientation. Also, magnetic circular dichroism was observed in $2p3d$ RIXS of Gd metal[9,10] recently. Similar magnetic circular or linear dichroism in $1s2p$ RIXS spectra should also be possible.

In the present analysis, we have simply assumed that the Fe $1s\rightarrow 3d$ excitation is due to the quadrupole transition. More detailed information on the relative strength of the Fe $1s\rightarrow 3d$ quadrupole and dipole transitions will be obtained from experimental measurements of the polarization dependence, as well as the scattering angle dependence, of the $1s2p$ RIXS, and their theoretical analysis in the near future.

ACKNOWLEDGMENT

The experiments at the NSLS were supported by the US-DOE under Contract No. DE-AC02-76CH00016. This work was partially supported by a Grant-in-Aid for Scientific Research from the Ministry of Education, Science, Sports and Culture in Japan. The computation in this work was done using the facilities of the Supercomputer Center, Institute for Solid State Physics, the University of Tokyo. The research of FdG has been made possible by the financial support of the Royal Netherlands Academy of Arts and Sciences (KNAW).

*Present address: Institut für Festkörperforschung, Forschungszentrum Jülich, 54245 Jülich, Germany.

†Present address: IPCMS-GEMM, UMR7503 CNRS, 23 Rue Du Loess, 67037 Strasbourg, France.

[1] J.-E. Rubensson, D. Mueller, R. Shuker, D. L. Ederer, C. H. Zhang, J. Jia, and T. A. Callcott, Phys. Rev. Lett. **64**, 1047 (1990).

[2] Y. Ma, N. Wassdahl, P. Skytt, J. Guo, J. Nordgren, P. D. Johnson, J.-E. Rubensson, T. Boske, W. Eberhardt, and S. D. Kevan, Phys. Rev. Lett. **69**, 2598 (1992).

[3] W. L. O'Brien, J. J. Jia, Q.-Y. Dong, T. A. Callcott, K. E. Miyano, D. L. Ederer, D. R. Mueller, and C.-C. Kao, Phys. Rev. Lett. **70**, 238 (1993).

[4] J. A. Carlisle, Eric L. Shirley, E. A. Hudson, L. J. Terminello, T. A. Callcott, J. J. Jia, D. L. Ederer, R. C. C. Perera, and F. J. Himpsel, Phys. Rev. Lett. **74**, 1234 (1995).

[5] S. M. Butorin, D. C. Mancini, J.-H. Guo, N. Wassdahl, J. Nordgren, M. Nakazawa, S. Tanaka, T. Uozumi, A. Kotani, Y. Ma, K. E. Myano, B. A. Karlin, and D. K. Shuh, Phys. Rev. Lett. **77**, 574 (1996).

[6] L.-C. Duda, G. Dräger, S. Tanaka, A. Kotani, J.-H. Guo, D. Heumann, S. Bocharov, N. Wassdahl, and J. Nordgren, J. Phys. Soc. Jpn. **67**, 416 (1998).

[7] K. Hämäläinen, C.-C. Kao, J. B. Hastings, D. P. Siddons, L. E. Berman, V. Strojanoff, and S. P. Cramer, Phys. Rev. B **46**, 14 274 (1992).

[8] M. H. Krisch, C.-C. Kao, F. Sette, W. A. Caliebe, K. Hämäläinen, and J. B. Hastings, Phys. Rev. Lett. **74**, 4931 (1995).

[9] W. A. Caliebe, C. C. Kao, L. E. Berman, J. B. Hastings, M. H. Krisch, F. Sette, and K. Hämäläinen, J. Appl. Phys. **79**, 6509 (1996).

[10] M. H. Krisch, F. Sette, U. Bergmann, C. Masciovecchio, R. Ver-

beni, J. Goulon, W. Caliebe, and C.-C. Kao, Phys. Rev. B **54**, R12 673 (1996).
[11] C.-C. Kao, W. A. Caliebe, J. B. Hastings, and J.-M. Gillet, Phys. Rev. B **54**, 16 361 (1996).
[12] F. Bartolomé, J. M. Tonnerre, L. Sève, D. Raoux, J. Chaboy, L. M. Garcia, M. Krisch, and C.-C. Kao, Phys. Rev. Lett. **79**, 3775 (1997).
[13] P. Kuiper, J.-H. Guo, L.-C. Duda, J. Nordgren, J. J. M. Pothuizen, F. M. F. de Groot, and G. A. Sawatzky, Phys. Rev. Lett. **80**, 5204 (1998).
[14] Y. Ma, K. E. Miyano, P. L. Cowan, Y. Aglitzkiy, and B. A. Karlin, Phys. Rev. Lett. **74**, 478 (1995).
[15] S. Tanaka and A. Kotani, J. Phys. Soc. Jpn. **62**, 464 (1993).
[16] Michel van Veenendaal and Paolo Carra, Phys. Rev. Lett. **78**, 2839 (1997).
[17] Eric L. Shirley, Phys. Rev. Lett. **80**, 794 (1998).
[18] Paolo Carra, Michele Fabrizio, and B. T. Thole, Phys. Rev. Lett. **74**, 3700 (1995).
[19] F. M. F. de Groot, M. Nakazawa, A. Kotani, M. H. Krisch, and F. Sette, Phys. Rev. B **56**, 7285 (1997).
[20] F. M. F. de Groot, Phys. Rev. B **53**, 7099 (1996).
[21] J.-J. Gallet, J.-M. Mariot, C. F. Hague, F. Sirotti, M. Nakazawa, H. Ogasawara, and A. Kotani, Phys. Rev. B **54**, 14 238 (1996).
[22] O. Brümmer and G. Dräger, Phys. Status Solidi **14**, K175 (1966).
[23] G. Dräger, R. Frahm, G. Materlik, and O. Brümmer, Phys. Status Solidi B **146**, 287 (1988).
[24] Tami E. Westre, Pierre Kennepohl, Jane G. DeWitt, Britt Hedman, Keith Hodgson, and Edward I. Solomon, J. Am. Chem. Soc. **119**, 6297 (1997).
[25] K. D. Finkelstein, Qun Shen, and S. Shastri, Phys. Rev. Lett. **69**, 1612 (1992).
[26] F. M. F. de Groot, J. Electron Spectrosc. Relat. Phenom. **67**, 529 (1994).
[27] W. A. Caliebe, C.-C. Kao, M. Krisch, T. Oversluizen, P. Montanez, and J. B. Hastings, in *Proceedings of the Tenth US National Conference on Synchrotron Radiation Instrumentation*, edited by Ernest Fontes, AIP Conf. Proc. No. 417 (AIP, New York, 1997).
[28] D. T. Cromer and D. Liberman, J. Chem. Phys. **53**, 1891 (1970).
[29] P. Kuiper, B. Searle, P. Rudolf, L. H. Tjeng, and C. T. Chen, Phys. Rev. Lett. **70**, 1549 (1993).
[30] R. D. Cowan, *The Theory of Atomic Structure and Spectra* (University of California Press, Berkeley, 1981).
[31] Raymond A. Bair and William A. Goddard, III, Phys. Rev. B **22**, 2767 (1980).
[32] James E. Hahn, Robert A. Scott, Keith O. Hodgson, Sebastian Doniach, Sylvia R. Desjardius, and Edward I. Solomon, Chem. Phys. Lett. **88**, 595 (1982).
[33] C. Brouder, J. P. Kappler, and E. Beaurepaire, in *Proceedings of the 2nd European Conference on Progress in X-ray Synchrotron Radiation Research, Rome, 1989*, edited by A. Balerna, E. Bernieŕi, and S. Mobilio (SIF, Bologna, 1990).